8 channel travelling wave coil array

Marco Müller[1], Reiner Umathum[1], Werner Wiesbeck[2], and Michael Bock[3]
[1]*Dept. of Medical Physics in Radiology, German Cancer Research Center (DKFZ), Heidelberg, Germany,* [2]*Dept. of Radiofrequency and Electronics, Karlsruhe Institute of Technology (KIT),* [3]*Dept. of Radiology, Medical Physics, University Hospital Freiburg, Freiburg*

Introduction

A travelling wave patch antenna concept was presented [1] as an alternative method for ultrahighfield MRI. This concept led to high global SAR and electromagnetic wave reflection in head and shoulder areas, or at the lower extremities. A recently presented coaxial coil setup [2] can focus the SAR, but B_1 erasement in the central propagation axis. In this work, we introduce a multifrequency 8-channel travelling wave RF array to solve these problems.

Materials and Methods

Coil: The coil array (length: 30cm; outer diameter: 30 cm) is based on a microstrip line design with 8 channels (width 6cm) (fig. 1), so it has no lower cut-off frequency as other travelling wave approaches, and can thus operate at multiple frequencies (e.g., for multi-nuclear MR). The outer copper surface acts as a RF shield with a segmented pattern to avoid eddy currents. The shield keeps the RF field inside the array and avoids coupling with the magnet bore. All microstrip line channels are designed to have 50 Ω impedance. The travelling RF waves are coupled into each strip line via 50 Ω coaxial cables with a relative phase difference of 22.5° to each other to provide a circularly polarized B_1 field. At the opposite coil end the remaining RF energy is coupled out via 8 coaxial cables and a power combiner, which leads the RF energy to a 50 Ω resistor. The power dividers and combiners are based on a Wilkinson design [3].

Phantom: A cylindrical phantom (diameter: 18cm; length: 80cm, acrylic glass) with 20l of a tissue equivalent solution at 300MHz according to the European standard EN 5036 was placed in the coil center. The dielectric parameters of the phantom fluid were measured at 300 MHz to $\varepsilon_R = 46.2$; $\sigma = 0.96$ S/m).

Measurements and simultations: B_1 maps were performed using a preconditioning-based flip angle mapping sequence (Siemens WIP package) [5] (TR: 2000ms; TE: 1.76ms, 240V excitation voltage) at 7 Tesla (Siemens Magnetom, Erlangen, Germany). RF nearfield measurements were performed with a robotic system (DASY52, SPEAG, Zürich, Switzerland) inside the phantom fluid at 300MHz (fig. 2, 3). The B_1, E- and SAR field distributions were evaluated and compared with FDTD field simulations (SEMCAD X V14.2, Speag, Zürich, Switzerland. In a next step field distributions of different dimensioned coils were evaluated with phantom simulations.

Imaging: ^{1}H imaging at 7 Tesla (GRE; TR: 90ms; TE: 2.4ms, 250V excitation voltage) was performed with the tissue equivalent phantom. Finally a human ex vivo leg was imaged with a 3D GRE sequence (Voxel size: 1*1*2mm³; TR: 7.0; TE: 3.1; TA: 5:23 min).

Whole body simulations: As a future prospect how B_1+ and SAR behavior of this concept with a human load could be whole body simulations with the virtual family model [5] Duke (male, 1.74m, 70kg) were performed (grid size: 172 million cells). Therefore the coil diameter was set to 450mm.

Results

S_{11} and S_{22} of the total arrangement including power dividers were lower than -24dB. Channel decoupling was better than-17dB at 300MHZ. RF measurements (fig.3) and simulations (fig.5) show a confining of the SAR inside the coil. At a distance of 5cm from the coil the measured SAR is reduced by more than 71% (fig.3). The deviation between measured and simulated B_1 profile in the phantom center is 5.4%. The SAR decreases towards the phantom center in the RF measurements / simulations by up to 99% / 96% (fig.2). In the human model simulation the SAR also decreases towards the central area by 98% (fig.5). Here the SAR is highest at the body surface. Inside the body area all simulated SAR values are smaller than in the surface region. The transversal B_1 characteristic of the RF measurements, the simulations and the measured B_1 maps show a B_1 decrease with a local field maximum in the coil center (fig.2, 4). The measured B_1 maps show a good correlation to the simulations and the RF measurements. In longitudinal orientation the RF measurements show a B_1 field deviation of 22% over a distance of 20 cm. At the coil center flip angles of 101° at 240V excitation voltage were measured, which corresponds to a B_1+ efficiency of $3.1\mu T \cdot kW^{-½}$. Fig. 6 shows the image of a human leg ex vivo (with severed foot) with a maximum FoV of 50 cm (voxel size: 1*1*2mm³; TR: 7.0; TE: 3.1; TA: 5:23 min).

Discussion and Conclusion

Simulations, RF measurements and MR imaging show that this travelling wave microstrip line array is usable for MRI at 7T. In comparison with other traveling wave concepts this array keeps the SAR inside the imaging region. It shows good longitudinal B_1 homogeneity and the positive aspect of an increasing B_1 field but a continuously decreasing SAR towards the center of the phantom (transversal). Simulations and measurements show that it is feasible to use this array design to mitigate the SAR hotspot problem. Compared to other traveling wave concepts this 8-channel travelling wave coil is fully pTx applicable and so the B_1 field characteristics could also be optimized. Finally this concept provides a simple, robust and cost-effective approach to perform spin excitation at UHF with SAR confining to the imaging area and additionally with a distinct SAR attenuation towards the central imaging area.

[1] Brunner et al, Nature 2009 **457**(7232) **[2]** Müller et al., Mag Res Med (early view), DOI: 10.1002/mrm.23069 **[3]** E. J. Wilkinson, IRE Trans.Microwave Theory Tech.1960; MTT–8:116–118 **[4]**Chung S et al, Magn Reson Med 2010;64:439–446 **[5]** Christ A et al, Phys Med Biol;55(2):N23-38

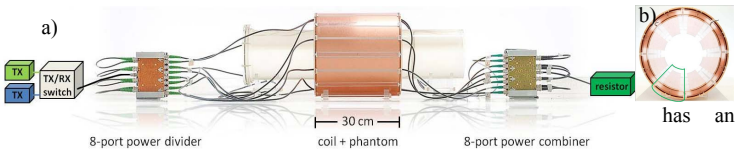

Fig. 1: a) setup of the 8-channel travelling wave coil with the tissue equivalent phantom. The power dividers/combiners are used if the scanner provides only one TX port. Otherwise the coil is fully pTx capable. b) front view without front shielding cover (green area marks one of the microstrip line channels.

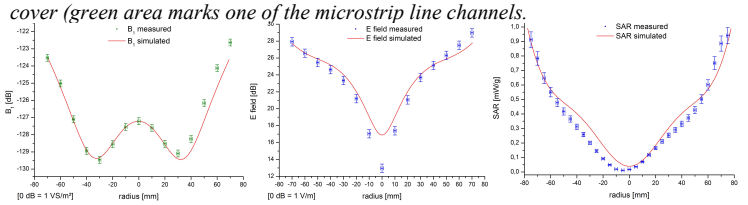

Fig. 2: Transversal profiles of the H_1, E and SAR field through the phantom center, measured by the DASY52 RF near field robotic system. For reference the red lines mark the according simulated field characteristics (values scaled by factor of 0.054).

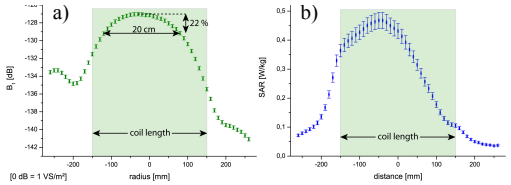

Fig. 3: a) Longitudinal H_1 field profile through the phantom center. b) averaged SAR within all transversal slices. The green rectangle marks the coil length.

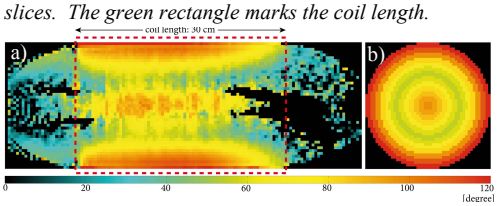

Fig. 4: B_1 maps of the phantom acquired at 7 Tesla (300 MHz) in longitudinal (a) and transversal (b) orientation. b) B_1 averaged over concentric rings of 6.8mm width.

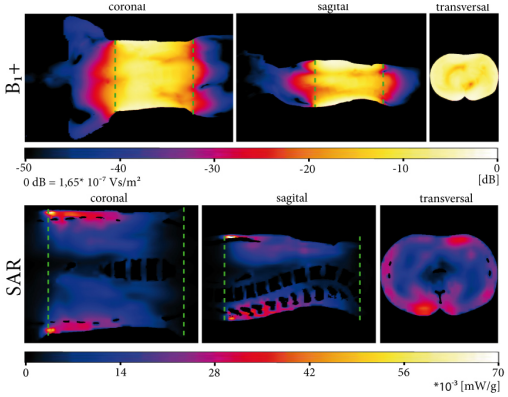

Fig. 5: simulated B_1+ and SAR field distributions of the human model (Duke). The green dotted lines indicate the coil dimensions.

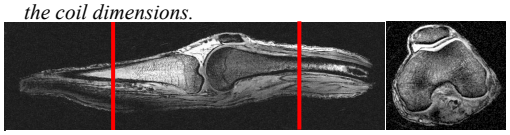

Fig. 6: Image of ex vivo knee in sagital and transversal orientation (Institute of Pathology, University of Heidelberg, Germany). Red lines indicate the coil limits. To achieve the maximum FoV of 50cm no coil front shielding covers are used.